Geochimica et Cosmochimica Acta Vol. 48, pp. 29–46
© Pergamon Press Ltd. 1984. Printed in U.S.A.

0016-7037/84/$3.00 + .00

"Fluffy" Type A Ca-, Al-rich inclusions in the Allende meteorite

GLENN J. MACPHERSON and LAWRENCE GROSSMAN[1]
Department of the Geophysical Sciences, University of Chicago, 5734 South Ellis Avenue, Chicago, Illinois 60637

(*Received April* 6, 1983; *accepted in revised form September* 28, 1983)

Abstract—Allende "fluffy" Type A's (FTA's) are a distinct sub-group of Ca-, Al-rich inclusions whose primary mineral assemblage consists of Al-rich melilite (Åk 0–33), spinel that is commonly very V-rich, perovskite and, frequently, hibonite. Some contain relatively coarse-grained melilite (up to 1.5 mm) that is intensely kink-banded and commonly reversely-zoned, hibonite and V-rich spinel. Others contain much finer-grained and strain-free melilite (≤50 μm) and have not been found to contain hibonite or V-rich spinel. Some FTA's contain both coarser- and finer-grained melilite and textural relationships indicate that the latter is replacing the former. FTA's are characterized by extremely irregular shapes and 60–75 volume per cent of fine-grained, secondary alteration products. Many are aggregates of innumerable nodules, each of which is surrounded by a Wark-Lovering-type rim sequence. These nodules are frequently separated from one another by matrix-like clastic rim material. Other FTA's do not have nodular structure. Structural and mineralogical characteristics of their Wark-Lovering rims suggest that FTA's did not achieve their shapes by deformation of a liquid or a hot, plastic solid. In contrast to those in Type B inclusions, formation of reverse zoning in the coarser-grained melilite crystals in FTA's cannot be understood in terms of crystallization from a liquid but are readily explainable by condensation from a solar nebular gas during a period of falling pressure. Further evidence against a liquid origin is the wide range of spinel compositions within individual coarser-grained FTA's. The fact that the reversely-zoned melilite crystals cannot have been produced in any kind of sublimation or distillation process precludes formation of these inclusions as volatilization residues. FTA's are aggregates in some of which are preserved vapor-solid condensate grains that formed at high temperature in the solar nebula.

INTRODUCTION

GROSSMAN (1975) classified coarse-grained, calcium-, aluminum-rich inclusions in Allende into two main varieties: Type A, characterized by abundant melilite and the absence of primary anorthite and titaniferous pyroxene; and Type B, characterized by abundant primary anorthite and pyroxene as well as melilite. Subsequent work showed that Type B's can be subdivided into two structural sub-types (WARK and LOVERING, 1977). MACPHERSON and GROSSMAN (1979) recognized two sub-groups of Type A inclusions. "Compact" Type A's have spheroidal to irregular shapes, 15–35% by volume of alteration products, V-poor spinel and melilite ranging in composition from Åk 10 to Åk 70. Some contain hibonite, but it occurs only near the outermost rims of the inclusions. Members of the other group have highly irregular and convoluted shapes, 60–75% alteration products, V-rich spinel and melilite ranging in composition from Åk 0 to ~Åk 35. Hibonite, when present, occurs scattered throughout the inclusions. We call the latter "fluffy" Type A's because, as will be shown herein, prior to their alteration and incorporation into the parent body, they were probably loosely-bound clumps of crystals drifting in the solar nebula, analogous to dustballs or snowflakes.

Even though GROSSMAN (1975), WARK and LOVERING (1976, 1978) and ALLEN *et al.* (1978) suggested that, of all coarse-grained inclusions, the best candidates for relict vapor-solid condensate grains may be found among the Type A's, no systematic study has ever been made of these objects to assess this possibility. The purpose of this paper is to do so, by describing and discussing the fluffy Type A's.

ANALYTICAL TECHNIQUES

Polished thin sections of all samples were studied optically and with a JEOL JSM-35 scanning electron microscope. Mineral analyses were obtained using an automated ARL-EMX-SM three-spectrometer electron microprobe, equipped with a Nuclear Semiconductor AUTOTRACE Si(Li) X-ray detector. Natural and synthetic minerals and glasses were used as standards. Wavelength dispersive analyses (w.d.a.) were done at 15 keV and a beam current of 0.5 μa. Energy dispersive analyses (e.d.a.) were done at 20 keV with a beam current of 0.1 μa. Data reduction for both methods was done by an on-line NOVA 2/10 computer. The program MAGIC (J. W. Colby, Bell Laboratories) was used for matrix corrections for w.d.a. while a program based on the procedure of REED and WARE (1973) was used for e.d.a. data reduction. The labelling system for each inclusion is the same as given in GROSSMAN (1975).

DESCRIPTIONS

Fluffy Type A inclusions are a group of irregularly-shaped, highly altered inclusions rich in gehlenitic melilite and spinel. Many contain hibonite and spinel that is rich in vanadium. Within this group of objects, however, there is a wide variety of inclusions differing from one another in texture and structure. One variant, illustrated in Fig. 1a, shows the highly irregular shape and aggregate structure typical of many of these inclusions. This variant is characterized by the relatively fine grain size (≤30 μm) of the melilite within the nodules. Another variant, also nodular, contains much coarser melilite (up to 1.5 mm) and is shown in Fig. 3. Within both of these inclusions, individual nodules are often mantled by a sequence of thin, mineralogically-distinct rim layers of the type described by WARK and LOVERING (1977), hereinafter called Wark-Lovering rims, which are the light-colored rinds in Fig. 1b.

[1] Also Enrico Fermi Institute, University of Chicago.

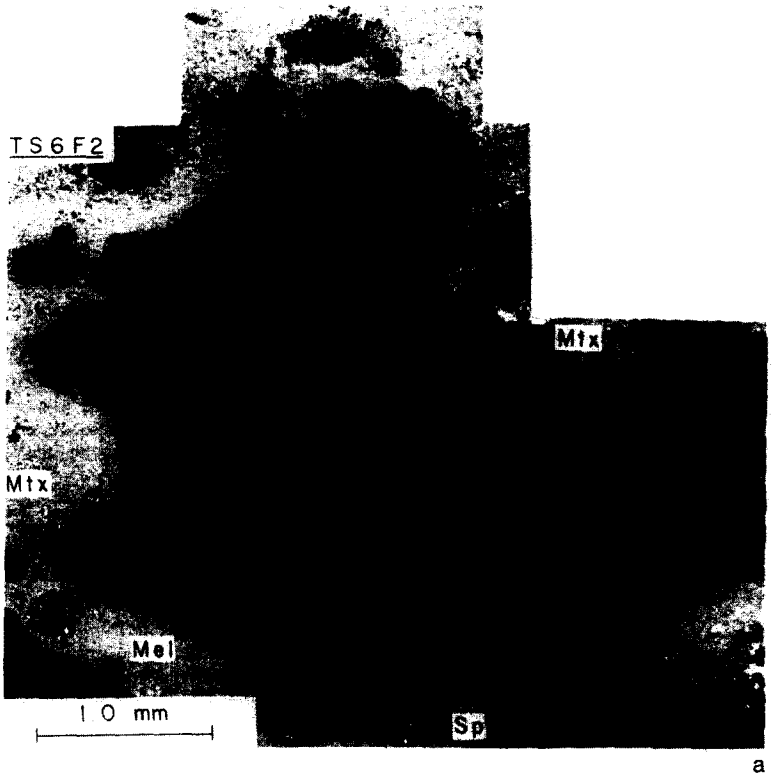

FIG. 1. (a) Back-scattered electron (b.s.e.) photomicrograph of inclusion TS6F2, showing its irregular shape and nodular structure. Abbreviations: Sp—spinel (dark), Mel—melilite (grey), Mtx—matrix. (b) Enlarged b.s.e. photomicrograph of TS6F2. Each nodule is surrounded by a light grey Wark-Lovering (W.-L.) rim. Interiors of nodules are partially altered to anorthite (An), nepheline (Ne) and grossular (Gr). Filling some of the internodular space is clastic rim material. Other abbreviations as in (1a) except: Hd—hedenbergite (white). (c) B.s.e. photomicrograph of a melilite-rich nodule in TS6F2, showing the fine-grained intergrowth of melilite with irregularly-shaped spinel grains. The exterior of the nodule, and large cavities within it, are mantled by a Wark-Lovering rim in which diopside (Di) is the most prominent phase. Fine-grained clastic rim material (C.R.) is visible at top left and top right. Other abbreviations as in (1a, b). (d) B.s.e. photomicrograph of a spinel-rich nodule in TS6F2. Note the irregular shapes of the melilite grains, implying that they formed after spinel. Abbreviations as used in (1a, b, c) except: Pv—perovskite, So—sodalite, Tr—troilite.

A third variant does not show the pronounced clumpiness seen in Fig. 1 but the mineralogy, mineral chemistry and intensity of alteration are identical to the clumpy ones and different from all other types of refractory inclusions. Wark-Lovering rims completely surround the outsides of inclusions of this type. In the nodular types, much of the material is fine-grained alteration products, the great abundance of which is probably due to the inclusions' high surface area-to-volume ratio that allowed the altering medium to saturate it thoroughly (MACPHERSON *et al.*, 1981). Even those that are not clumpy are intensely altered, suggesting that they originally had porous, aggregate structures like the clumpy ones, a property that implies that none of the fluffy Type A's were ever totally molten. Some fluffy Type A's, including both nodular and non-nodular varieties, contain both the fine and coarser melilite crystals noted above. In these, it is reasonably clear that the fine-grained melilite is replacing the coarser melilite.

Filling interstices between many of the rimmed nodules and completely mantling the outsides of many entire inclusions (see Fig. 6a) is a thick (200–300 μm) "clastic" rim sequence like that described by MACPHERSON and GROSSMAN (1981b). Around the outsides of inclusions, this clastic rim is continuous and unbroken like the Wark-Lovering rim, but differs from it in being highly variable in thickness. The thickest portions are those filling topographic depressions and pockets on the surfaces of inclusions. Mineralogically and texturally, these clastic rims resemble the Allende matrix which encloses them, but have well defined layers that differ from each other and from the Allende matrix in their grain size, modal mineral proportions and mineral chemistry.

Although we have examined more than twenty fluffy Type A's (hereafter FTA's), what follows are detailed descriptions of only eight of them, selected to illustrate the great variety of textures and structures within this class of objects.

TS6F2 and TS1F7

TS6F2 (Fig. 1a) is an example of a nodular type containing fine-grained melilite. It is approximately 0.4 cm in overall dimension but is actually an aggregate of many, small (70–600 μm), rounded to irregularly-shaped bodies (Fig. 1b). The interior of each of these small nodules consists of an intergrowth of melilite, spinel and perovskite, but the relative proportions of these phases vary greatly from nodule to nodule. In many nodules, such as the one shown in Fig. 1c, the dominant phase is melilite which forms dense aggregates of polygonal crystals ($\leqslant$30 μm) within which are enclosed rounded to irregularly-shaped spinel grains ($\leqslant$3 μm) and rounded cavities (1–5 μm). Rare additional phases may include perovskite and troilite (both $\leqslant$ 1 μm). Although the fine grain size in these nodules makes paragenetic inferences difficult, it appears that spinel and perovskite crystallized before melilite. Other nodules, such as the one shown in Fig. 1d, consist largely of

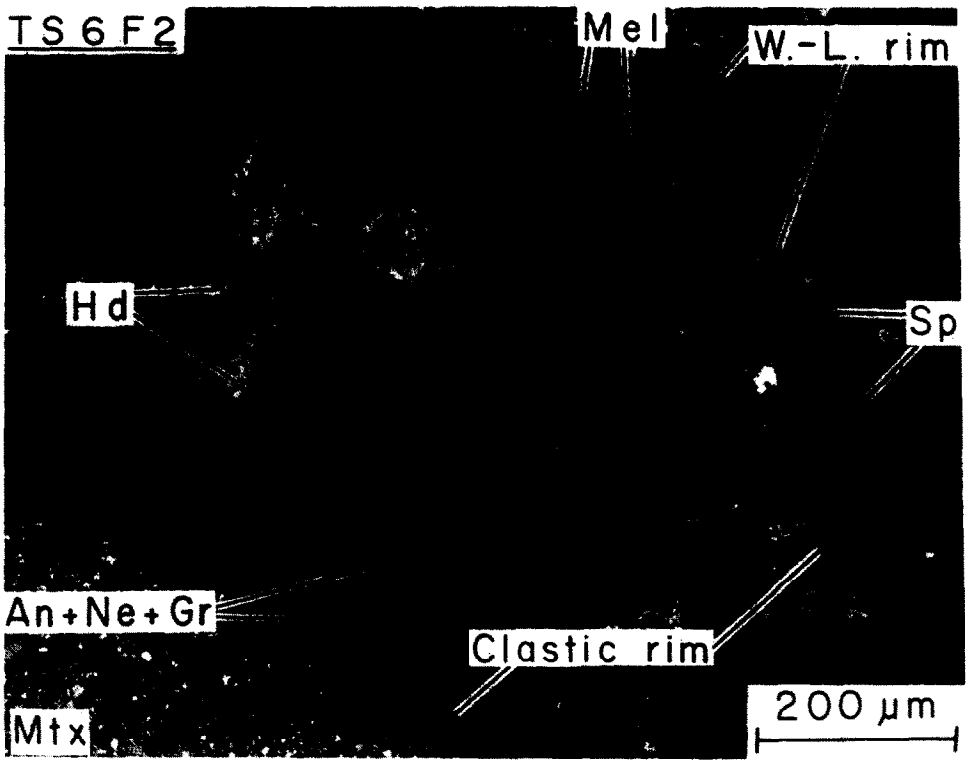

FIG. 1. (Continued)

densely packed spinel grains of uncertain size with sparse, irregularly-shaped patches of melilite (⩽20 μm), rounded to irregular cavities (⩽10 μm) and rare troilite (⩽1 μm) and perovskite (⩽10 μm) grains. The occurrence of perovskite within spinel grains and of melilite interstitial to spinel indicates that the crystallization sequence was probably perovskite before spinel before melilite. These spinel-rich nodules are similar in their textures, sizes and mineralogy to some refractory spherules in the Murchison C2 chondrite (MACDOUGALL, 1981; MACPHERSON *et al.*, 1983a) but differ from the latter in containing no hibonite. The spinel-rich nodules are more like spinel-rich, melilite-bearing, rimmed nodules which we have found very rarely in the interiors of pink fine-grained Allende inclusions (WARK and LOVERING, 1977). Still other nodules consist mostly of fine-grained (5–10 μm) secondary phases that are apparently replacing melilite: anorthite with lesser grossular, nepheline and sodalite. All of the nodules are mantled by rim layers consisting of, from innermost to outermost, fassaite + sparse Fe-rich spinel, anorthite + nepheline + sodalite, aluminous diopside and hedenbergite, *i.e.*, Wark-Lovering rim sequences. In addition, relatively large cavities in the interiors of the nodules are lined with Wark-Lovering rim sequences, suggesting that the cavities are re-entrants. Finally, as noted previously, the nodules are separated from one another in many places by clastic rim material.

Figure 2a is a back-scattered electron (b.s.e.) photograph of TS1F7, another nodular-structured inclusion with fine-grained melilite. The most frequently encountered FTA's are closer in size to TS1F7, ~1.2 mm in length, than to TS6F2, leading to the general conclusion that Type A's are smaller than Type B's on average (GROSSMAN, 1975). This may be

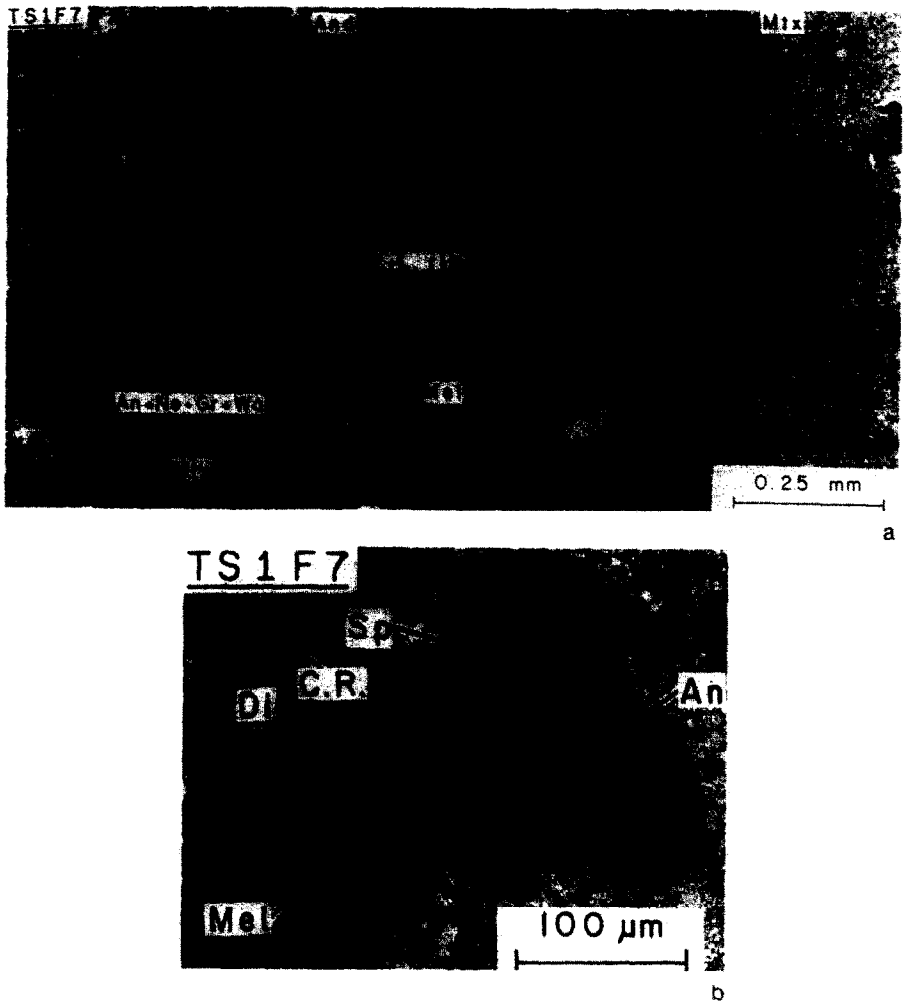

FIG. 2. (a) B.s.e. photomicrograph of TS1F7, showing its nodular structure, the continuity of the Wark-Lovering rim around each nodule and the differences in mineral proportions from nodule to nodule. The large dark nodule at top center is mostly spinel, while other nodules are rich in melilite. Abbreviations as in Fig. 1 except: And—andradite (white), Wo—wollastonite. (b) B.s.e. photomicrograph of a nodule in TS1F7, showing a fine-grained intergrowth of melilite and spinel. The melilite is partially altered to anorthite. The nodule is mantled by a diopside rim and clastic rim material. Abbreviations as used previously.

due to preferential fragmentation of Type A's, supporting our contention that the fluffy Type A's are aggregates and thus more friable than the Type B's which are solidified melt droplets. The primary phases in TS1F7 are melilite, spinel and perovskite but, like TS6F2, the relative proportions of these phases vary greatly from nodule to nodule. Furthermore, as seen in Fig. 2b, textures in the nodules of this inclusion are very similar to those in TS6F2. The modal variability within both inclusions is not thought to be a thin-sectioning effect: no one of the nodule types could be sliced up in different ways to produce such apparent disparate abundances. It is thus possible that the different types of nodules within a single inclusion are not cognate but, rather, solidified independently of one another and that the inclusions originated as loosely-bound aggregates of these nodules. Further evidence for this is that each of the nodules in both inclusions is individually mantled by a Wark-Lovering rim sequence which probably formed by reaction of the solar nebular gas with surfaces of the nodules (MACPHERSON *et al.*, 1981), implying that the inclusions were so porous during rim formation that the gas had free access to the surfaces of all the constituent nodules.

TS24F1

TS24F1 is the largest FTA in our collection (2.5 cm in length), is highly irregular in shape and has a nodular structure and relatively coarse-grained melilite. It is shown in its entirety in GROSSMAN (1980). Its structure consists of a contorted, irregularly-shaped, massive central object surrounding which are many rounded to angular nodules (0.25–~3 mm). An enlarged SEM view of a portion of the inclusion is shown in Fig. 3. Each nodule, and also the central object itself, is individually mantled by nearly continuous Wark-Lovering rims. In the outer parts of the inclusion, some of the nodules are separated from each other not only by their rims but also by intervening strings of clastic rim material. Neighboring "island" nodules have their own complete Wark-Lovering rims and, in two dimensions, appear to be attached to the rest of the inclusion only by means of the clastic rim which may act as a kind of cement (MACPHERSON and GROSSMAN, 1981b). Alternatively, the coarse-grained material in the "islands" may be contiguous in the third dimension with coarse-grained material in the rest of the inclusion.

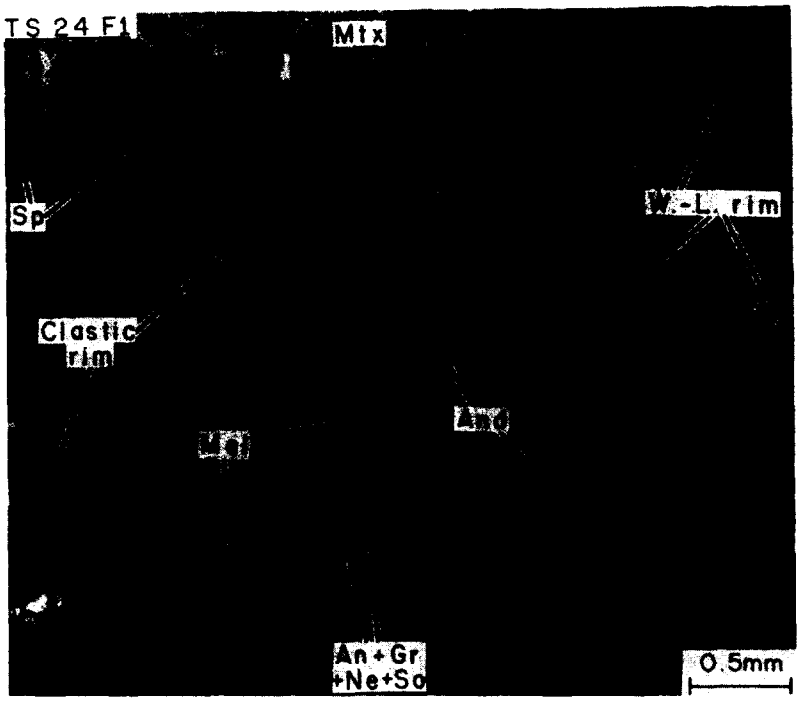

FIG. 3. B.s.e. photomicrograph of a portion of TS24F1, showing its nodular structure. Its outer surface, near the top of the photo, is overlain by a light-colored clastic rim that is thickest in topographic pockets. This clastic rim material also fills internodular spaces. Abbreviations as used previously.

The interiors of the core and nodules consist of one or more large crystals of melilite. Other, less abundant primary phases are spinel ± hibonite ± perovskite. All nodules contain anorthite + nepheline + grossular + sodalite as fine-grained secondary phases. The inclusion's core and some larger nodules have numerous, polycrystalline melilite-rich regions separated from each other by wide expanses of secondary phases. Within the inclusion are two textural varieties of melilite: relatively large (up to ~1.5 mm) blocky crystals which are highly kink-banded and smaller (≤50 μm) equant crystals that are tightly interlocked in a mosaic-like texture and which are relatively strain-free. Commonly, the mosaic-textured melilite regions partially mantle large kink-banded melilite crystals, suggesting that the finer-grained melilite is replacing the coarser-grained melilite.

Spinel occurs mostly as rounded to euhedral grains within melilite and is very inhomogeneously distributed. Some melilite grains have very few spinel inclusions, others are densely packed with spinel grains and still others may be densely crowded with spinel inclusions in one place but spinel-free elsewhere. There is a tendency for spinel inclusions to be more densely concentrated in gehlenite-rich melilite crystals or portions of melilite crystals than in åkermanite-rich crystals or portions thereof, as seen in the reversely-zoned melilite in Fig. 4. No spinel framboid structures such as seen by EL GORESY *et al.* (1979) were found. The spinel is not uniform in its optical properties: pink spinel in the inclusion's rim sequence is iron-rich, pale orange spinel in the inclusion interior is vanadium-rich and colorless spinel in the inclusion interior is lacking in significant quantities of minor elements (see MINERAL CHEMISTRY). Orange, vanadium-rich spinel is noteworthy because it has not been observed in compact Type A or Type B inclusions, but is apparently common in FTA's. Hibonite occurs as small (≤35 μm) bladed crystals, either enclosed by melilite or as large polycrystalline aggregates surrounded by alteration phases. In the former mode of occurrence, the hibonite is euhedral even when in contact with spinel. Hibonite grains in the latter mode of occurrence tend to be somewhat ragged in appearance relative to those enclosed in melilite, a feature also noted by ALLEN *et al.* (1978) in CG-11. Perovskite occurs as small (≤10 μm) grains in the Wark-Lovering rim sequence, as larger (≤200–300 μm), rarer, irregularly-shaped grains in the inclusion interior that are occasionally enclosed completely within melilite, as small (≤10 μm) euhedral crystals decorating the surfaces of spinel grains within melilite and as aggregates of irregularly-shaped crystals intergrown with hibonite and secondary alteration phases. In places, these aggregates are enclosed by melilite. When the large, irregular grains are surrounded by alteration products, they generally have thin (≤5 μm) rims of dark, grey-green fassaite. Fremdlinge (EL GORESY *et al.*, 1978) have not been found in TS24F1 and noble metal nuggets are very rare. Melilite seems to be the phase most commonly replaced by alteration products. At the contacts with alteration products, melilite has highly irregular and embayed outlines. Fractures within melilite are commonly filled with grossular.

Figure 5 shows a portion of the outer surface of TS24F1. Altered melilite is overlain by a Wark-Lovering rim sequence which, in turn, is overlain by a clastic rim sequence. Outside of the clastic rim is Allende matrix. Not shown in this photo is that the clastic rim mantles the entire periphery of the inclusion. This observation, plus the sedimentary-like texture of the clastic rim as described by MACPHERSON and GROSSMAN (1981b), indicates that the clastic rim was deposited on the inclusion prior to aggregation of the Allende parent body, possibly while the inclusion was drifting freely in space. A microfault has produced an offset in the Wark-Lovering rim sequence and places melilite in direct contact with clastic rim material. Where the clastic rim directly overlies the fault, the innermost layers (I, II in Fig. 5) thin out and might be interpreted as having been faulted. The outermost layer (III in Fig. 5), however, is clearly not cut because the trace of its contact with the matrix continues unbroken across the plane of the fault. The faulting thus occurred either before deposition of the entire clastic rim sequence or at least before deposition of the outermost clastic layer. Because of this, both faulting

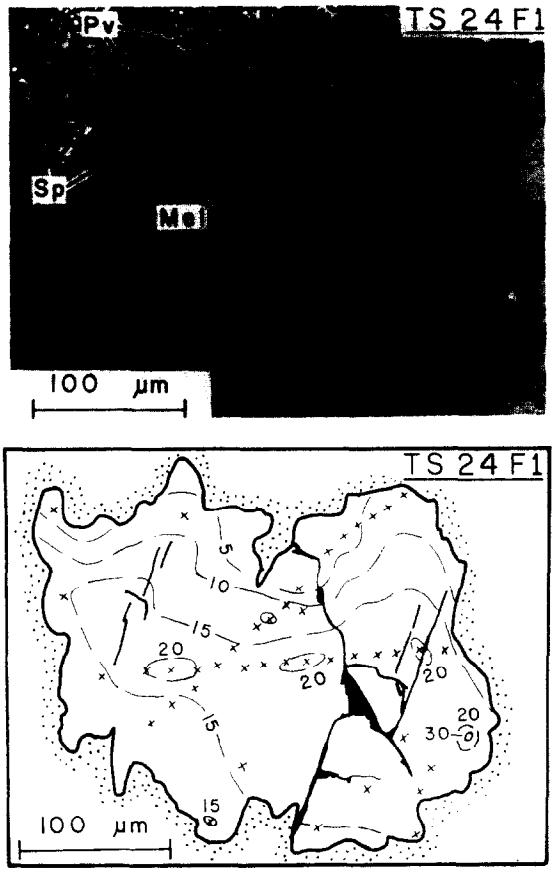

FIG. 4. B.s.e. photomicrograph (a) and line drawing (b) of a melilite crystal in TS24F1. Spinel inclusions are concentrated near the top of the crystal in this photo, a region shown in (b) to be part of the gehlenite-rich outer margin of this reversely-zoned crystal. Contours are mole % åkermanite, in 5 mole % intervals. Crosses indicate the locations of microprobe analyses used to construct the contours. The small, localized, high-åkermanite area at far right is due to a perovskite inclusion at depth in the host melilite. This and similar perovskite grains have pyroxene rims, and apparently have reacted with the melilite to produce pyroxene + åkermanite-rich melilite.

and deposition of the Wark-Lovering rim occurred prior to completion of deposition of the clastic rim and, hence, prior to incorporation of TS24F1 into the parent body.

TS27F1

TS27F1 (Fig. 6a) is a pear-shaped inclusion, ~3 × 4 mm in size, with a concentric structure. It is not nodular and contains both the coarser- and finer-grained melilite types. The core consists of fine-grained secondary phases and is surrounded by an intermediate zone containing fine- and coarse-grained primary melilite + spinel + hibonite + perovskite, followed by an outer mantle containing the same fine-grained secondary phases as the core. The entire inclusion is mantled by a Wark-Lovering rim similar to those described previously and, finally, by a clastic rim ~ 50–300 μm thick that is continuous and unbroken around ~75% of the inclusion. As in other refractory inclusions, the clastic rim is thickest where it fills topographic depressions on the inclusion's surface.

Figure 6b is an enlarged b.s.e. photomicrograph of one coarse-grained region, showing a few large (~200–400 μm) melilite crystals that are severely kink-banded, though the latter feature is not visible in the photo. These poikilitically enclose euhedral spinel grains (<25 μm), hibonite blades (10–20 μm), rare perovskite grains (~25 μm) and Ni-Fe and Os-Ru metal beads (<5 μm). The two types of metal beads do not touch one another. Mantling this coarse-grained area is a dense, fine-grained intergrowth of polygonal and strain-free melilite crystals (~10 μm), irregularly-shaped spinel grains (~5 μm) and perovskite crystals (~1–6 μm). Figure 6c is an enlarged transmitted-light photomicrograph taken with crossed polarizers, showing the transition between the coarse- and fine-grained melilite. Towards the contact, each of the large melilite crystals breaks up into many small ones, and some of the smaller melilite crystals are actually enclosed within the large crystals. Coarse- and fine-grained melilite has the same chemical composition (Åk~0–11). Textural relationships between the coarse- and fine-grained melilite-rich portions of this inclusion indicate that the coarse-grained assemblage is being replaced by the granular assemblage. The sugary texture of the latter, with its polygonal crystals and 120° triple grain junctions, is more suggestive of solid state recrystallization than of crystallization from a melt. The heating that caused recrystallization may have been due to the shock event that deformed the coarse melilite crystals or to an unrelated, later event.

TS28F1 and TS29F1

TS28F1 is a highly altered oblong inclusion, approximately 3.5 mm in maximum dimension, that does not have a nodular structure. It has a concentrically zoned distribution of mineral

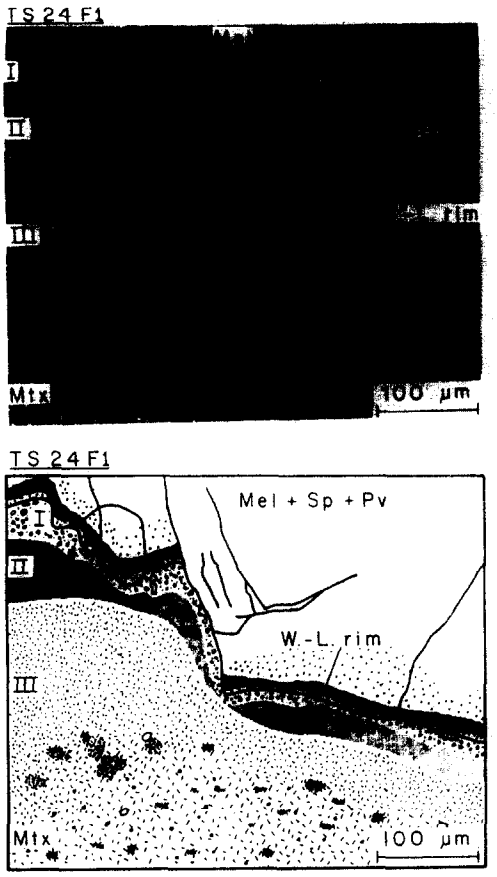

FIG. 5. B.s.e. photomicrograph (a) and line drawing (b) of a portion of the surface of TS24F1, showing a microfault that cuts the Wark-Lovering rim but not clastic rim layer III and probably not layer I or II. Notation for layers I–III corresponds to that in MACPHERSON and GROSSMAN (1981b). Abbreviations as used previously.

phases. The sole primary phase in the core of TS28F1 is hibonite which occurs as a few abnormally large (≤0.25 mm) crystals surrounded by abundant secondary nepheline, anorthite, grossular and an unknown iron-rich aluminous phase. The hibonite shows strong yellow to colorless pleochroism in most places but the crystals also have small patches which are nearly colorless. These patches are much poorer in Mg and Ti than the strongly colored variety (see MINERAL CHEMISTRY). Surrounding this central region, and separated from it by a wide band of alteration material, is a mantle of melilite (14–200 μm), hibonite, perovskite, colorless spinel and rare grains of deep orange-red, V-, Fe-rich spinel. These primary phases in the mantle tend to occur in clumps separated from one another by fine-grained, secondary anorthite and grossular, and which are largely absent from the interiors of the clumps. Melilite, the most abundant phase in clumps, has a polygonal habit, resulting in 120° triple grain junctions. Unlike other FTA's, the melilite even in these polygonal mosaics is kink-banded. Spinel is not abundant but, where present, occurs as inclusions within melilite. Hibonite is, in places, intimately intergrown with melilite. Outside of this relatively coarse-grained region is more secondary alteration material and, finally, a Wark-Lovering rim.

TS29F1 consists of two separate fragments in the thin section, one a rounded piece, 2 mm in diameter, and the other an oblong piece, ~0.5 × 1.5 mm in size. The two pieces are separated by ~0.25 mm of Allende matrix in the plane of the thin section. The surfaces of both pieces lack Wark-Lovering rim sequences in places. This inclusion is not nodular and contains relatively coarse melilite. It is thus mineralogically and texturally similar to TS28F1 but lacks the concentric structure. Hibonite is unevenly distributed and is primarily concentrated in a few clusters, in one of which the blades, intergrown with spinel and melilite, are radially oriented about a common center. This inclusion is the only FTA in which we have found spinel framboids (EL GORESY *et al.*, 1979). These consist of small rings of spinel and interstitial perovskite grains, enclosed within melilite, whose centers contain partially altered melilite.

CG-11

CG-11 was described in detail by ALLEN *et al.* (1978) and trace element data are given in DAVIS *et al.* (1978). It consists of several isolated nodules in thin section which, prior to excavation from the original slab surface, merged into one large inclusion, ~7 mm in length. Like other FTA's described above, CG-11 contains: 1) no Fremdlinge and only rare noble metal beads; 2) orange-colored, vanadium-rich spinel in addition to colorless, vanadium-poor spinel; and 3) two textural varieties of melilite crystals, one being coarse-grained and highly kink-banded and the other finer-grained, more equant and more strain free. One unusual feature of CG-11 is the presence of a cluster of seven, large (≤90 μm), highly titaniferous pyroxene crystals that are neither in the rim nor associated with perovskite and are confined to one end of only one nodule, rather than distributed evenly throughout the inclusion. The crystals poikilitically enclose spinel, are locally intergrown with melilite and are surrounded by alteration products. Titaniferous pyroxene is common as a rim on perovskite in this and other FTA's, but isolated large crystals like the ones in CG-11 are rare. The melilite grains in CG-11 show rather well defined reverse zoning (see MINERAL CHEMISTRY), having rims with higher Al/Mg ratios than the cores.

TS25F1

This very large (~0.5 × 1.5 cm) and oblong inclusion does not have the nodular structure seen in previous inclusions. Although there are deep embayments into the inclusion that are filled by clastic rim material, there are no fragments completely enclosed within such rims. The inclusion is highly altered and many large melilite crystals and clusters of crystals are completely isolated within extensive, porous regions of secondary phases including nepheline, anorthite, grossular, sodalite and wollastonite needles. The unique feature that distinguishes TS25F1 from all other FTA's in our collection is the presence of numerous large complex Fremdlinge, up to ~100 μm in size. These generally rounded bodies consist mostly of Ni-Fe metal, V-Fe oxide, Fe-Ni sulfide and Ca-phosphate. Many occur as inclusions within melilite. Some smaller metal beads are enclosed within spinel. In all other FTA's we have examined, Fremdlinge are absent and metal nuggets are rare.

Hibonite in TS25F1 tends to be concentrated into a few large clusters of small (15–30 μm) blades. One cluster is almost completely enclosed within a mantle of melilite crystals. Some hibonite crystals are completely enclosed within individual melilite crystals, implying that hibonite formed before melilite. Hibonite is locally intergrown with spinel and, in such occurrences is euhedral (Fig. 7). The largest melilite crystals in TS25F1 (≤0.6 mm) are rectangular in shape and intensely kink-banded. Some of these are reversely-zoned, and the composition profiles of one such crystal are shown in Fig. 8 (see MINERAL CHEMISTRY). All the melilite crystals contain inclusions of spinel and, less commonly, perovskite, hibonite, Fremdlinge and metal beads. As was noted for TS24F1, there tends to be an increased concentration of spinel inclusions in the most gehlenite-rich portions of melilite crystals. As in other FTA's, spinel enclosed in melilite ranges from colorless and vanadium-poor to orange and vanadium-rich. The most intensely orange spinel grains are enclosed by alteration products and are associated with hibonite.

Surrounding the inclusion is a thick and well-developed Wark-Lovering rim, mantled in turn by a clastic rim. The innermost part of the clastic rim consists of blocky olivine crystals, many of which occur as donut-shaped rings that enclose metal grains or sulfide grains. These olivine structures are identical to some seen in amoeboid olivine aggregates (BAR-MATTHEWS *et al.*, 1979). In fact, the olivine grains in the rim of TS25F1 are locally concentrated into large clusters that look like pieces of amoeboid olivine aggregate inclusions attached to the rim of the FTA.

Similar objects

EL GORESY *et al.* (1980) described an inclusion (15/10 I) that, in some respects, resembles our FTA's and may be a member of this group. It has a concentrically-zoned structure with (1) an aggregate core consisting of numerous spherical nodules, angular clasts and individual crystals; (2) a mantle of large kink-banded melilite crystals; and (3) a Wark-Lovering rim. Although 15/10 I is similar to FTA's in having an aggregate structure and a spinel-, melilite-, hibonite-rich composition, it differs from our nodular inclusions in having a melilite mantle which surrounds the aggregate of nodules, in having a Wark-Lovering rim enclosing the entire inclusion rather than individual nodules and in having angular clasts exhibiting "rhythmic layering" (EL GORESY *et al.*, 1980). Our non-nodular FTA's do not contain concentric spherical bodies or angular clasts.

We have one inclusion with characteristics reminiscent of some of those of 15/10 I, and it is shown in Fig. 9a. Labelled TS12F5, it has a core consisting of spinel-centered rimmed objects (Fig. 9b) like those in Allende fine-grained inclusions (*e.g.*, WARK and LOVERING, 1977), along with numerous individual crystals of pyroxene and feldspathoids. Mantling this core is a discontinuous band containing mostly melilite, spinel and fine-grained alteration products (Fig. 9c). The outside edge of the inclusion is mantled by a poorly-developed Wark-Lovering rim. Thus, it is similar to 15/10 I in having an aggregate core surrounded by a melilite-rich mantle and a Wark-Lovering rim all the way around the inclusion but different in containing no hibonite and no angular clasts with rhythmic layering.

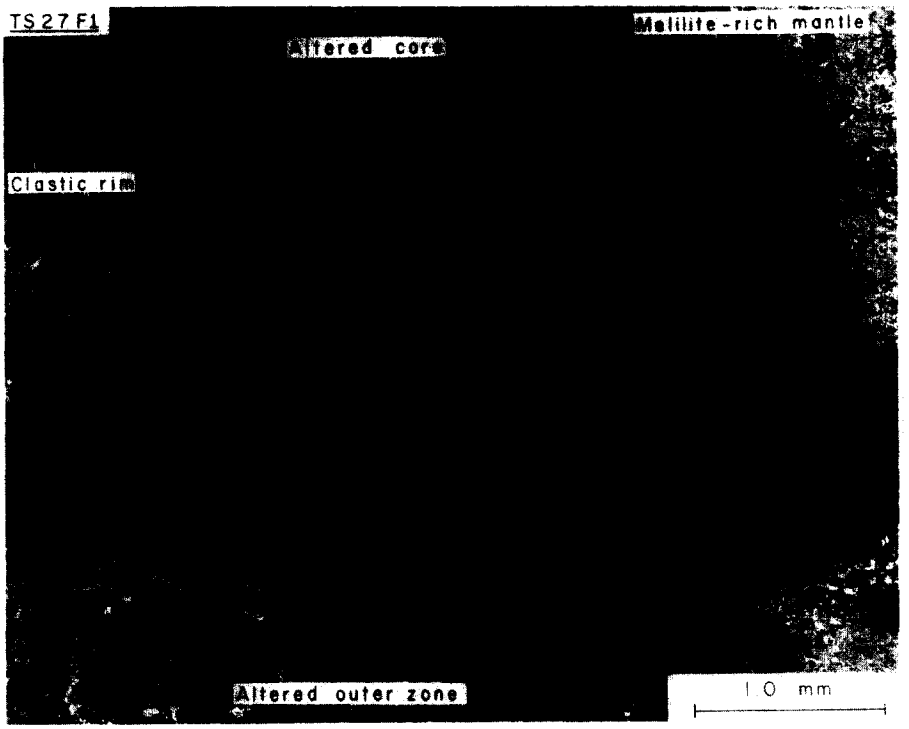

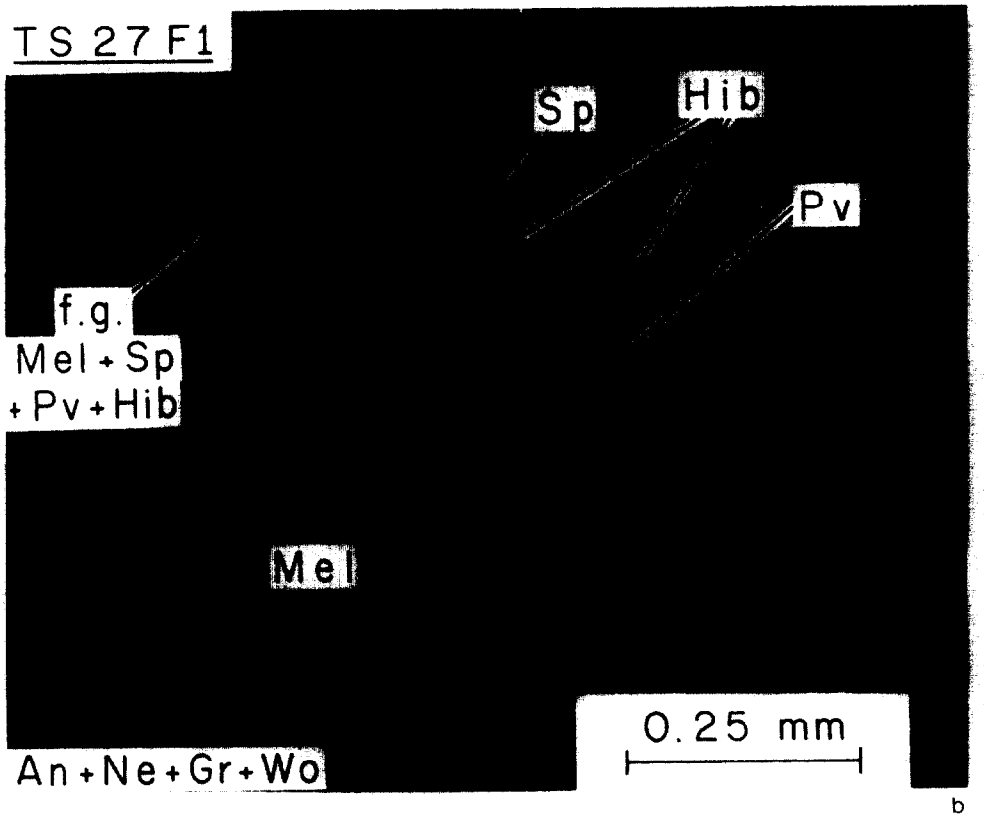

FIG. 6. (a) B.s.e. photomicrograph of TS27F1, showing concentric structure. (b) Enlarged b.s.e. photomicrograph of coarse-grained portion of melilite-rich mantle. Note equant spinel in center, enclosed with hibonite (Hib) and perovskite inside large melilite crystals. Surrounding this assemblage is a fine-grained (f.g.) intergrowth of the same phases. Abbreviations as used previously. (c) Transmitted light photomicrograph, taken with polarizers crossed, showing transition between large melilite crystal and fine-grained aggregate of polygonal melilite crystals.

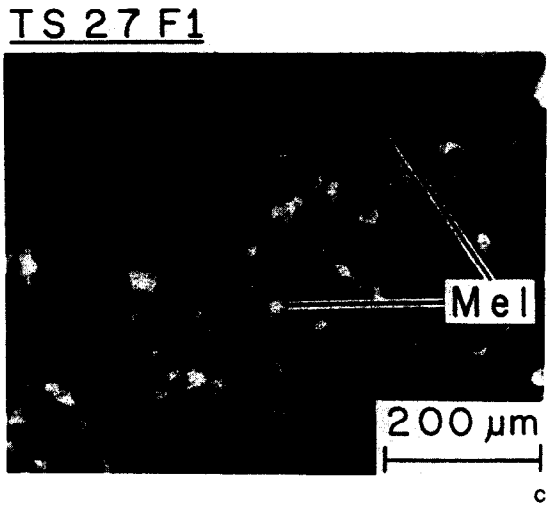

FIG. 6. (Continued)

Neither 15/10 I nor TS12F5 precisely resembles any of our FTA's, nor are they identical with fine-grained inclusions. Objects such as these may be a link between the melilite-rich FTA's and the melilite-poor fine-grained inclusions.

MINERAL CHEMISTRY

Because of the difficulty of obtaining contamination-free analyses from inclusions containing fine-grained primary phases, all of our hibonite and spinel analyses are from inclusions containing relatively coarse-grained material. The narrow composition range and aluminous character of the melilite as well as the high vanadium content of the spinel distinguish FTA's from other refractory inclusion types in Allende. The chemistry of secondary phases in FTA's is similar to that in other Allende inclusions. This subject will not be treated here, but is discussed in ALLEN *et al.* (1978).

Melilite

Figure 10 shows the range in gehlenite content of melilite from a number of FTA's compared with the observed ranges for melilite from all compact Type A's and Type B's in our collection. Melilite from all FTA's shows a more limited composition range, Åk ~ 0–33, than that in the latter two inclusion types. Melilite in FTA's is also distinctive in two other ways. First, there is no relationship between the composition of a melilite grain and its spatial location within the host inclusion in any of our FTA's. In many B's and compact A's, however, melilite grains near inclusion margins are more aluminous (gehlenite-rich) than those near inclusion cores. Second, some melilite crystals in at least five of our FTA's are reversely-zoned, being more gehlenite-rich in their rims than in their cores. This was demonstrated previously in the case of CG-11 by ALLEN *et al.* (1978). Those authors noted a difficulty in inferring the zoning pattern of the original melilite crystal because subsequent secondary alteration had obscured the grain boundaries. In Fig. 8, we give composition profiles for a melilite grain in TS25F1. In the present case, we have much better control on the original size and shape of the crystal because it is closely bounded on three sides by neighboring melilite grains. It is clear that the åkermanite-rich (Åk ~ 22) zone really is at the core of the crystal and that the gehlenite-rich rim (Åk 5–8) does extend all the way around the periphery. For many other melilite crystals in this and other FTA's, unfortunately, the original crystal boundaries are not so clear and it is thus not certain whether reverse zoning is characteristic of all of those crystals. One useful property that allows these zoning patterns to be observed optically is the birefringence of aluminum-rich melilite which is very sensitive to small differences in composition and which increases with increasing Al/Mg ratio.

The minor element contents of melilite from all our FTA's are very low. Energy dispersive analyses of many grains did not show any Na, K, Fe, Ti and Mn which, if present, are thus at or below the 0.5% level. Analyses done by wavelength dispersion on CG-11 gave the following upper limits (2σ): K_2O < .02%, Na_2O < .03%, FeO < .06% and TiO_2 < .05% (ALLEN *et al.*, 1978).

Spinel

Spinel in FTA's shows a wide spectrum of compositions even within single inclusions. Analyses of several examples are given in Table 1. No evidence for non-stoichiometry of the kind discussed by EL GORESY *et al.* (1983) was found in these inclusions, as deviations from ideal cation sums are thought to be within our analytical uncertainty. The major component in all FTA spinel is $MgAl_2O_4$, but many contain appreciable amounts of FeO and V_2O_3. V_2O_3 contents of 1.5% and higher are common in spinel from FTA's, whereas V_2O_3 seldom exceeds 0.5% in spinel from other coarse-grained inclusion types. Iron-rich spinel (several per cent FeO or more) tends to be pink in transmitted light and occurs only in the Wark-Lovering rim sequence and within or near zones of intense secondary alteration in inclusion interiors, suggesting that iron was introduced into the spinel during alteration of the host inclusions. Some iron-rich spinel in the interiors of inclusions is also vanadium-rich (Table 1, #1) and the most vanadium-rich spinel is very iron-rich (Table 1, #2). Although this might suggest that vanadium was carried into the inclusions in the same secondary process responsible for the iron, there is no consistent correlation of FeO with V_2O_3, contrary to the observations of EL GORESY *et al.* (1980). For example, some spinel grains enclosed completely within melilite contain up to ~2% V_2O_3 but are virtually iron-free (Table 1, #3). There is also no correlation between vanadium content of spinel and proximity of spinel to alteration zones. For example, some spinel grains within alteration veins that cross-cut melilite are lower in vanadium than others located away from veins and enclosed in the same melilite crystal. Also, spinel crystals in Wark-Lovering rims on FTA's are iron-rich but vanadium-poor (ALLEN *et al.*, 1978). Finally, even though all refractory inclusions are altered, only FTA's have vanadium-rich spinel.

For these reasons, we conclude that vanadium in FTA spinel is primary in origin. This conclusion implies that the large variations in vanadium contents of different spinels

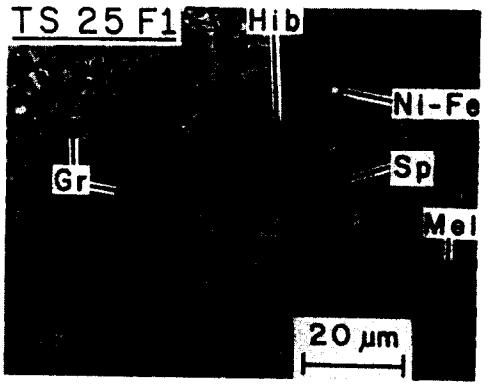

FIG. 7. B.s.e. photomicrograph showing an intergrowth of spinel and hibonite in TS25F1. Note that the hibonite blades are euhedral, and that the shape of the spinel is entirely subordinate to that of the hibonite. Both phases are enclosed within melilite that is partially altered to grossular. Abbreviations as used previously except: Ni-Fe—nickel-iron metal.

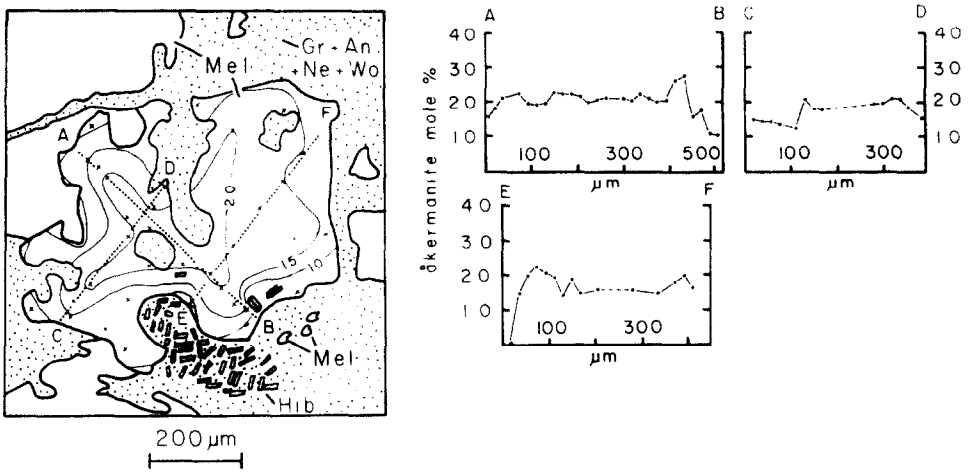

FIG. 8. A melilite crystal in TS25F1 showing reverse zoning. Contours are mole % åkermanite, in 5 mole % intervals. Also shown are composition profiles determined by electron microprobe along the traverses indicated by the dotted lines across the crystal. Small crosses are locations of additional microprobe analyses. Note bordering melilite crystals at top and bottom left and right edge.

within the same FTA preclude wholesale equilibration during any kind of igneous or high-temperature metamorphic event (see DISCUSSION). A problem does remain in explaining why the *most* vanadium-rich spinel is also the most iron-rich. One possibility is that vanadium-rich spinel was more susceptible to secondary introduction of iron than vanadium-poor spinel.

Hibonite

Analyses of several hibonite grains from FTA's are given in Table 2. These span nearly the entire range of compositions of meteoritic hibonite reported by KEIL and FUCHS (1971). The blue-luminescent, orange-pleochroic, Mg-, Ti-rich variety is most common. The orange-luminescent, colorless, Mg-, Ti-poor variety is rarer and can be found as patches within Mg-, Ti-rich crystals (see Table 2, #1, 2). Similarly-zoned crystals were reported by KEIL and FUCHS (1971). The principal trace component in FTA hibonite is V_2O_3, falling in the range ~0.3–2.5% in the inclusions studied herein. EL GORESY *et al.* (1980) reported 0.2–3.3% V_2O_3 in hibonite in inclusion 15/10 I. Vanadium seems to be directly correlated with titanium and magnesium and inversely correlated with aluminum, suggesting that it substitutes for aluminum in the hibonite structure. The vanadium is therefore probably present as V^{3+}. Deviations from ideal cation sums fall within our analytical uncertainties and are thus not thought to be due to non-stoichiometry effects such as claimed by EL GORESY *et al.* (1980, 1983).

ORIGIN OF FLUFFY TYPE A'S

Much of the interest in refractory inclusions in carbonaceous chondrites is due to their mineralogical and chemical similarity to the highest-temperature, vapor-to-solid condensates predicted to have formed in the primordial solar nebular cloud (GROSSMAN, 1972; LATTIMER and GROSSMAN, 1978). The intriguing possibility exists, therefore, that there are mineral grains preserved in some of these inclusions that actually condensed as solids from the solar nebular gas. This possibility has been cast in doubt by the proposal that some or all of the refractory inclusions have passed through a liquid stage at some time in their history, either because the original condensates were later melted (KURAT, 1970) or because matter originally condensed as metastable liquids (BLANDER and FUCHS, 1975). We intend to show in the following section that at least some refractory inclusions, the fluffy A's, are aggregates and have never experienced wholesale melting as did many Type B's. Such a conclusion was reached by EL GORESY *et al.* (1980) for 15/10 I, an inclusion similar in some respects to FTA's. If FTA's were never molten, they would be the best candidates in which to look for products of direct vapor-to-solid condensation from the solar nebula.

Evidence from Wark-Lovering rims

On first glance, it would seem that the highly irregular shapes and nodular structures of many FTA's could not possibly have formed if the inclusions were ever molten. In fact, however, it is conceivable that molten or at least highly plastic droplets were deformed by impact and quickly frozen to retain lobate shapes. This might have occurred either during incorporation of FTA's into the Allende parent body or earlier while the inclusions drifted freely in space. Evidence against models of this class stems from the Wark-Lovering rim sequences, one of which is seen wrapping around a very convoluted portion of the surface of TS24F1 in Fig. 3. Deformation could not have occurred after these rims were deposited. The first argument is based on their shapes. If deformation had occurred after rim deposition and if the rims were rigid while the interior was plastic, the rims would be broken in many places and would not conform so faithfully to the convoluted shapes of the inclusion, particularly in those places with very small radii of curvature. If, on the other hand, the rims were also plastic at the time of deformation, the rim would be expected to be consistently thicker at bends in the surface than along its straight

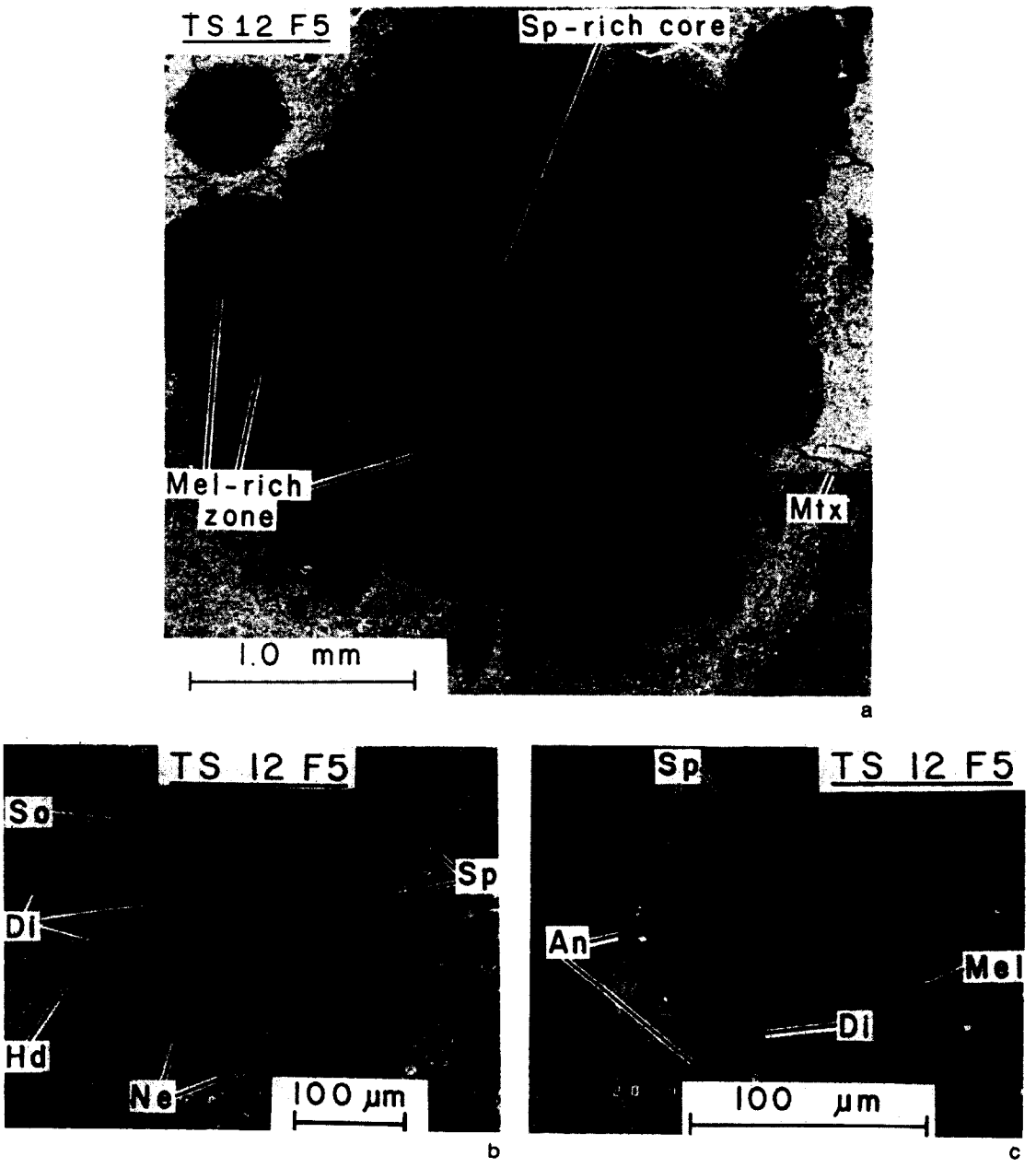

FIG. 9. (a) B.s.e. photomicrograph of TS12F5, showing its concentrically-zoned structure. (b) Enlarged b.s.e. photomicrograph of the spinel-rich core of TS12F5. Spinel crystals are individually mantled by rims of diopside and, in places, hedenbergite. Interstices are either voids or filled with nepheline and sodalite. Abbreviations as used previously. (c) Enlarged b.s.e. photomicrograph of the melilite-bearing mantle of TS12F5. Melilite is partially altered to anorthite and diopside. Spinel grains are enclosed within melilite, and, where excavated by alteration of the melilite, do not show the rimmed structure seen in the spinel-rich core (9b) of TS12F5. Abbreviations as used previously.

portions. In fact, no such consistent relationship is found. The rim does not vary greatly in thickness anywhere on the inclusion, ranging from ~10–15 μm and most commonly being ~10–30 μm. We conclude that rims were deposited on surfaces which were already highly convoluted. The second argument is based on mineralogy. NORD *et al.* (1982) found hedenbergite in contact with nearly pure wollastonite in the rim of TS24F1. Because this assemblage is unstable relative to bustamite + hedenbergite above 775°C, they conclude that the rim formed below this temperature. Since this is far below the solidus temperature of a liquid having the bulk composition of an FTA, 1360°C (J. R. BECKETT, unpub. data), we conclude that FTA's were neither molten nor plastic both during and after rim deposition. As we have already seen, formation of the Wark-Lovering rim occurred prior to incorporation of the inclusions into the Allende parent body.

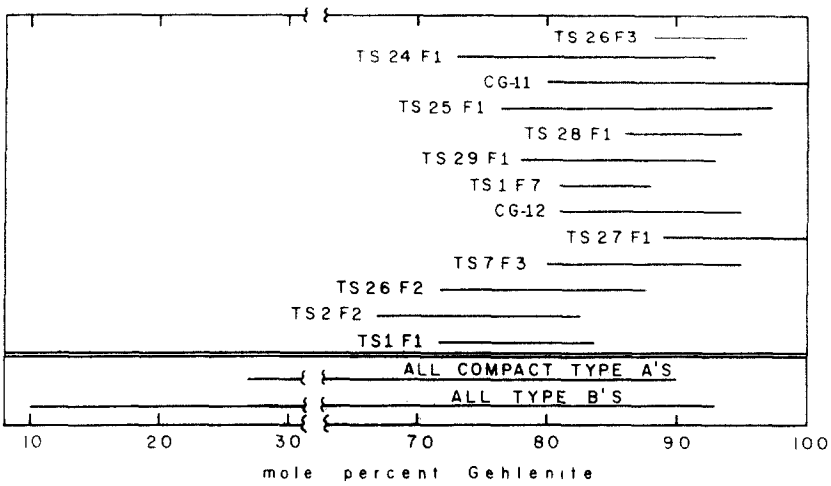

FIG. 10. Melilite composition ranges within individual fluffy Type A inclusions compared with total melilite composition ranges in Type B and compact Type A inclusions.

Thus, if the inclusions underwent plastic deformation, this also took place prior to incorporation. In this case, however, it is hard to imagine how an impact energetic enough to deform a droplet and even produce myriad subdroplets (as would be required to form nodular FTA's like TS6F2) would not also completely scatter those droplets over great distances. If we assume instead that the nodules in TS6F2 and other similar objects are in fact attached to one another in the third dimension (out of the plane of the thin section), then an impact model would require that the lobes froze before the liquid relaxed back into a sphere. We thus conclude that *no* model involving a wholesale molten stage can satisfactorily account for the shapes of FTA's.

The above arguments, however, leave open the possibility that individual nodules may have been molten prior to their aggregation into FTA's. Because of the textural relations between finer- and coarser-grained melilite seen in inclusions such as TS27F1 and TS24F1, we have inferred above that the relatively fine-grained material has replaced the coarser-grained material in a solid-state recrystallization process. For this reason, inclusions such as TS6F2 and TS1F7 that are composed entirely of the finer-grained material are least likely to preserve information bearing on the condensation process. We therefore turn our attention to those inclusions and their constituent nodules that contain coarser-grained melilite and other phases.

TABLE 1

Electron microprobe analyses of spinel from fluffy Type A inclusions in Allende

	1	2	3	4	5	6
	TS25F1	TS28F1	TS24F1	TS24F1	TS27F1	TS52F1
SiO_2	n.a.†	n.a.	0.77	0.07	0.15	0.22
Al_2O_3	67.88	61.32	67.70	69.20	71.21	69.71
TiO_2	0.13	0.06	0.30	0.32	0.13	0.22
MgO	25.09	12.00	27.81	28.67	27.71	28.63
FeO	4.01	20.67	0.06	0.07	1.72	0.20
CaO	n.a.	n.a.	1.20	0.33	0.42	0.51
V_2O_3	1.63	4.91	2.28	0.79	0.93	0.60
Cr_2O_3	0.15	0.20	0.21	0.18	n.a.	n.a.
Total	98.89	99.16	100.33	99.63	102.27	100.09
	Cations per 4 oxygens					
Mg	0.918	0.478	0.990	1.022	0.968	1.016
Fe	0.082	0.462	0.001	0.001	0.034	0.004
Ca	---	---	0.031	0.008	0.010	0.013
Al	1.963	1.930	1.907	1.951	1.968	1.956
Cr	0.003	0.004	0.004	0.003	---	---
V	0.032	0.105	0.044	0.015	0.017	0.011
Si	---	---	0.018	0.002	0.003	0.005
Ti	0.002	0.001	0.005	0.006	0.002	0.004
Total Cations	3.000	2.980	3.000	3.008	3.002	3.009
	Detection limits for minor elements (3σ , in wt.% oxide)					
TiO_2	0.04	0.02	0.04	0.04	0.04	0.04
FeO	0.04	0.03	0.04	0.04	0.03	0.03
Cr_2O_3	0.04	0.02	0.04	0.04	---	---
V_2O_3	0.03	0.02	0.03	0.03	0.01	0.01

All analyses by wavelength dispersion.
†n.a. - not analyzed.

Evidence from crystallization sequences

Individual hibonite crystals in FTA's are commonly enclosed within melilite grains, and clusters of hibonite crystals are surrounded by polycrystalline mantles of melilite. These features indicate that hibonite began to crystallize prior to melilite and pose a problem for any model interpreting coarser-grained FTA's as once-molten objects, as results of experimental studies are incompatible with an origin of these inclusions by solidification from melts. Although the bulk compositions of coarser-grained FTA's (BECKETT *et al.*, 1980) plot well within the melilite phase volume in the experimentally determined system CaO-MgO-Al_2O_3-SiO_2 and, indeed, crystallization of a liquid of this composition yields melilite as the first-crystallizing phase (BECKETT and GROSSMAN, 1982), hibonite formed *before* melilite in the actual inclusions. In fact, hibonite has not even been found among the experimental run products but anorthite, a primary phase not found in actual FTA's, is produced synthetically.

An observation cited by KORNACKI (1982) as evidence that refractory inclusions are not preserved relics of vapor-solid condensation is the occurrence of spinel

TABLE 2

Electron microprobe analyses of hibonite from fluffy Type A inclusions in Allende

	1	2	3	4	5	6	7
	TS28F1†	TS28F1†	TS25F1	TS29F1	TS27F1	TS24F1	TS52F1
SiO_2	0.36	0.15	1.39	0.26	0.72	0.23	1.15
Al_2O_3	89.25	83.14	79.84	84.40	81.70	80.29	87.44
TiO_2	1.37	5.25	6.09	3.80	4.18	5.82	1.19
MgO	0.86	2.60	2.82	2.17	3.78	3.25	1.17
FeO	0.04	0.02	0.08	n.d.*	0.08	0.14	0.05
CaO	8.12	7.36	8.86	8.22	8.55	8.64	8.60
Cr_2O_3	0.02	0.03	0.05	n.d.	n.a.††	n.a.	n.a.
V_2O_3	0.31	0.52	0.94	0.31	0.46	0.77	0.12
Sc_2O_3	<0.02	<0.02	n.a.	n.a.	0.04	0.05	0.04
Total	100.33	99.07	100.07	99.16	99.51	99.19	99.76
	Cations per 19 oxygens						
Ca	0.968	0.895	1.073	0.997	1.038	1.058	1.032
Mg	0.143	0.440	0.475	0.367	0.640	0.553	0.194
Al	11.695	11.113	10.640	11.259	10.918	10.812	11.533
Ti	0.115	0.448	0.518	0.323	0.356	0.500	0.100
Fe	0.004	0.002	0.008	---	0.007	0.013	0.005
Cr	0.002	0.003	0.004	---	---	---	---
V	0.028	0.047	0.085	0.028	0.042	0.070	0.011
Sc	---	---	---	---	0.004	0.005	0.003
Si	0.040	0.017	0.157	0.030	0.081	0.026	0.128
Total Cations	12.995	12.965	12.960	13.004	13.086	13.037	13.006
	Detection limits for minor elements (3σ, in wt.% oxide)						
FeO	0.02	0.02	0.02	---	0.03	0.03	0.03
Cr_2O_3	0.02	0.02	0.02	---	---	---	---
V_2O_3	0.02	0.02	0.01	---	0.01	0.01	0.01
Sc_2O_3	0.02	0.02	---	---	0.03	0.03	0.03

Analyses 1-3, 5-7 by wavelength dispersion; 4 by energy dispersion.
†Analyses 1 and 2 are from different parts of a single crystal in TS28F1.
*n.d. - not detected by energy dispersive analysis.
††n.a.- not analyzed.

enclosed poikilitically within melilite, indicating that spinel formed before melilite. This order is the reverse of the sequence predicted by equilibrium condensation theory (LATTIMER and GROSSMAN, 1978) but, for many refractory inclusions (Type B's), is in agreement (BECKETT *et al.*, 1980) with the crystallization sequence predicted by liquid-solid phase equilibria in the system CaO-MgO-Al_2O_3-SiO_2. What is not generally recognized, however, is that this cannot be used to argue that an origin of coarser-grained FTA's by crystallization from a melt is more likely than an origin by vapor-solid condensation because the bulk compositions of these objects plot in the melilite phase volume (BECKETT *et al.*, 1980), making melilite, not spinel, the first-crystallizing phase from a liquid with the composition of an FTA. The problem is that the observed poikilitic texture is inconsistent with *both* models. In order to reconcile the texture with an origin by vapor-solid condensation, it must be argued that the predicted condensation sequence is inapplicable in some way.

FEGLEY (1982) suggested that the absence of $CaAl_4O_7$ from all but one known refractory inclusion (CHRISTOPHE *et al.*, 1982) poses a serious difficulty for simple vapor-solid condensation models for the origin of these inclusions. This was based on calculations he performed which predicted that $CaAl_4O_7$ would form by equilibrium reaction of hibonite with the solar nebular gas at ~1650°K at 10^{-3} atm. total pressure. Fegley's argument is weakened, however, by two possible problems. First, his calculations employ free energy data for $CaAl_4O_7$ obtained by ALLIBERT *et al.* (1981) who cite a recommended value intermediate between their two determinations which differ by ~5 kJ/mole. ALLIBERT *et al.* (1981) pointed out that their data are in excellent agreement with those of some other workers but are ~17 kJ/mole more negative than thermochemical data of KOEHLER *et al.* (1961). If $CaAl_4O_7$ were only 6.1 kJ/mole less stable than the value recommended by ALLIBERT *et al.* (1981), it would disappear completely from the calculated condensation sequence (J. M. LATTIMER, unpub. data). Second, FEGLEY's (1982) calculations are limited to thermodynamic data for pure $CaAl_{12}O_{19}$ whereas, except for that in the unique inclusion HAL (ALLEN *et al.*, 1980) and an isolated hibonite fragment in the H3 chondrite Dhajala (BISCHOFF and KEIL, 1983), meteoritic hibonite always contains significant MgO and TiO_2 in solid solution (KEIL and FUCHS, 1971; ALLEN *et al.*, 1978; MACPHERSON *et al.*, 1983a). The presence of these components would certainly expand the stability field of hibonite relative to $CaAl_4O_7$ which apparently accepts very little MgO or TiO_2 into solid solution (CHRISTOPHE *et al.*, 1982). For these reasons, $CaAl_4O_7$ may not be an equilibrium condensate from a solar gas.

In summary, although the crystallization sequence of spinel and melilite remains an unresolved problem for both the liquid crystallization and vapor-solid condensation models, experiments on crystallization of hibonite from melts are inconsistent with the former model and arguments against the latter model are not compelling. On balance, we favor an origin for coarser-

grained FTA's by condensation of solids from the solar nebula.

Evidence from melilite composition and zoning

MACPHERSON and GROSSMAN (1981a) described a Type B1 inclusion in which the melilite crystals have gehlenite-rich cores and åkermanite-rich rims. In addition, individual crystals around the periphery of the inclusion are gehlenite-rich at the inclusion edge and become progressively more åkermanite-rich along their length toward the inclusion core. These melilite zoning features can be readily explained in terms of the crystallization of this inclusion from a molten droplet. In the system gehlenite-åkermanite (OSBORN and SCHAIRER, 1941), complete solid solution exists between the end-members and a minimum occurs in the liquidus at Åk ~ 73. During crystallization on the aluminum-rich side of this minimum, both liquid and crystals become progressively enriched in magnesium relative to aluminum with falling temperature. Under most circumstances, this is true even in the presence of additional components (CHINNER and SCHAIRER, 1962; GEE and OSBORN, 1969). Thus, in a molten droplet that cools by radiation from its surface, it is expected that early-formed melilite crystals will be gehlenite-rich and concentrated near the droplet margin and that, as a result of further cooling, the crystals will be progressively more åkermanite-rich both parallel and perpendicular to their long axes. These are essentially the features preserved in the above inclusion.

GEE and OSBORN (1969) showed that an exception to this general trend of melilite composition with temperature can occur when the onset of voluminous crystallization of another phase causes the Al/Mg ratio of the residual liquid to rise abruptly. In the system gehlenite-åkermanite-diopside-anorthite, they predicted that reverse zoning of melilite should occur not only on the Mg-rich side of the melilite minimum but also in a limited range of bulk composition on the Al-rich side close to the minimum where clinopyroxene co-crystallizes with melilite before crystallization of anorthite. MACPHERSON *et al.* (1983b) showed experimentally that reverse zoning indeed occurs in some Type B inclusions when anorthite suppression causes co-crystallization of melilite and pyroxene and suggested that this effect can thus occur even in very gehlenite-rich bulk compositions. In other Type B's, such as the one mentioned above, co-crystallization of anorthite with melilite negated the effect of later clinopyroxene crystallization on the liquid composition, resulting in normally-zoned melilite.

Reversely-zoned melilite in the coarser-grained FTA's, however, cannot be so easily explained in terms of crystallization from a melt. First, clinopyroxene does not appear during crystallization of a liquid of this bulk composition (BECKETT and GROSSMAN, 1982). Second, no phase or combination of phases that co-crystallizes with melilite in such melts causes the Al/Mg ratio of the liquid to rise sufficiently to reverse the zoning in the melilite, as all the melilite produced in these experiments is unzoned (J. R. BECKETT, unpub. data).

We can envision only one other plausible way of increasing the Al/Mg ratio of such a liquid during crystallization, preferential volatilization of Mg and Si from it. Isothermal volatilization of a melt droplet containing spinel and melilite of composition Åk 20 would cause the composition of melilite in equilibrium with the melt to become more gehlenitic, assuming melilite remains stable through the change in composition of the melt. Reverse zoning would not be the result of establishment of a diffusion profile within the original crystals because coupled cation substitution involving tetrahedral sites is sluggish. Rather, it would be due to overgrowth of new melilite upon the residual crystals of Åk 20. The change in composition of the melilite would be accompanied, however, by resorption of spinel as magnesium is lost from the system relative to aluminum. Thus, if such a process were responsible for the reverse zoning, the abundance of spinel crystals in the liquid coexisting with the melilite would decrease and the reversely-zoned rims that might crystallize from this liquid would be expected to enclose a lower density of spinel grains than the cores of the same melilite crystals. In fact, as discussed above and shown in Fig. 4, spinel inclusions are often most abundant in the gehlenite-rich rims of FTA melilite, exactly the opposite of what would be predicted. We conclude that, if coarser-grained FTA's were once molten, reverse zoning in their melilite was not caused by an increase in the Al/Mg ratio of the liquid during crystallization.

A totally different way of producing reverse zoning in a liquid-crystal system has been demonstrated by LOFGREN (1974). He found that supercooling of liquids of plagioclase composition caused rapid crystal growth, precipitation of plagioclase less anorthitic than the equilibrium composition for that temperature and approximately isothermal reverse zoning by as much as 8 mole per cent. Because of the topological similarity between the plagioclase phase diagram and the Al-rich part of the melilite one, similar behavior would be expected for melilite. Since the difference between liquidus and solidus temperatures is considerably larger in the plagioclase system than in the melilite system, however, the extent of reverse zoning would probably be less for melilite than for plagioclase and thus insufficient to produce the 15 mole per cent observed in TS25F1. Furthermore, upon continued cooling, a normally-zoned outer mantle would be expected to form on top of the reversely-zoned regions, a feature not observed in FTA melilite. We thus conclude that reversely-zoned melilite crystals in FTA's are not the result of supercooling of melts.

Rapid heating followed by preferential, rapid volatilization of magnesium and silicon from totally molten droplets at constant temperature may be a means

of producing effective supercooling in the sense that the liquid could find itself metastably within the melilite + liquid phase volume. If reversely-zoned melilite crystals form, they will again have normally-zoned outer margins if cooling begins prior to total consumption of the liquid. Also, only a few mole per cent of reverse zoning would be expected. Both of these predicted features are contrary to observations. Because of this and the absence from FTA's of evidence for resorption of spinel, which would be expected in all models involving preferential volatilization of magnesium, we conclude that reversely-zoned melilite in FTA's did not form by rapid heating followed by rapid preferential volatilization of magnesium and silicon from melts.

An apparently simple mechanism for producing the observed reverse zoning is isochemical heating of a system composed of liquid and melilite of composition Åk 20. Assuming that the pre-existing melilite does not melt, crystals like those observed in TS25F1 could only be produced if the temperature reaches 1550°C, where the equilibrium melilite composition is Åk 5. The major problem is, however, that, in this temperature range, melting is so rapid that the cores of Åk 20 would begin to melt if superheated by as little as 10°, allowing reverse zoning of only ~5 mole per cent, from Åk 20 to Åk ~ 15. To reach 1550°C where the outermost zone would be Åk 5, requires the cores to be superheated by 70°, at which point they would melt, producing a spongy texture which is not observed. Even if the cores do not melt, a normally-zoned region outside of the reversely-zoned one would be expected to form upon cooling of the melt, another feature which is not observed. Thus, the reverse zoning in FTA melilite could not have been caused by isochemical heating of a liquid-crystal mixture.

There remains one possibility for producing reverse zoning if the melilite crystallized from a melt, a change in the externally controlled pressure. In general, however, a very large pressure change is required to produce an appreciable change in the composition of a solid solution phase in equilibrium with a melt at constant temperature. In the plagioclase liquid-solid system, for example, the equilibrium composition dependence on pressure is ~0.5% An/10^3 atm. (LINDSLEY, 1968) and on water pressure is ~1% An/10^3 atm. (YODER *et al.*, 1957). Although such data do not exist for the melilite system, the magnitudes of the effects are probably similar. Kilobar-scale increases in pressure would be required to reverse the zoning of a crystallizing melilite by even 1–2 mole % åkermanite at constant temperature. It is hard to imagine how such changes in gas pressure could have been achieved in the early solar system, as physical models of a two solar mass nebula do not allow pressures to exceed 10^{-1} atm. We are thus unable to reconcile the reverse zoning of the melilite with any model for the origin of coarser-grained FTA's that involves crystallization from a melt.

We have seen that it is very unlikely that FTA's crystallized in their entirety from liquid droplets and that the mineralogical compositions of at least the coarser-grained FTA's are difficult to interpret in terms of crystallization from a melt, suggesting that even individual nodules within these aggregates may not have crystallized from melt droplets. In this section, the evidence presented from melilite zoning patterns argues strongly that the latter suggestion is correct. Further support for the idea that many of the individual nodules were not molten stems from our observation that there is no relationship between the compositions of melilite crystals and their spatial positions within either individual nodules or, for that matter, even entire inclusions as exists in, for example, the Type B1 inclusion discussed by MACPHERSON and GROSSMAN (1981a). The lack of such a relationship does not in itself preclude an origin by liquid crystallization but the existence of such a relationship in inclusions known to have been molten makes a once-molten origin for coarser-grained FTA's less likely.

On the other hand, if neither these whole inclusions nor their constituent nodules crystallized from melt droplets but, instead, are aggregates of vapor-solid condensates, a relationship between melilite composition and spatial position would not be expected. Furthermore, there is a ready explanation for reverse zoning in melilite in models in which FTA's condense as solids from the solar nebular gas. This is based on the fact that the pressure changes necessary to alter the composition of a solid solution phase at a given temperature are much smaller in gas-solid than in liquid-solid equilibria. ALLEN and GROSSMAN (1978) suggested that a small decrease in nebular pressure during condensation of melilite is capable of producing the reverse zoning observed in CG-11. This is illustrated in Fig. 11 which is from full equilibrium, solar nebular condensation calculations exactly like those whose results appeared in LATTIMER and GROSSMAN (1978), except that an updated set of thermodynamic data were used which included data for calcium aluminates. At all pressures, there exists a temperature interval of 75° within which the åkermanite content of the melilite increases from near-zero to more than 50% as the temperature falls. The temperature at which any particular åkermanite content is reached falls with the total pressure. The melilite grain shown in Fig. 8 has a core of Åk 22 and a rim of Åk 8. It is seen in Fig. 11 that the core of this grain could have formed in equilibrium with the solar nebular gas at ~1458°K at a total pressure of 10^{-3} atm. The rim of this crystal could have formed at the same temperature as the core if the melilite continued to grow during a gradual drop in pressure of only 30%, to ~7×10^{-4} atm. Alternatively, if the temperature was falling during continued growth of the rim of the melilite grain, the drop in pressure required to produce the observed zoning would have to be greater than in the isothermal case, *e.g.*, about 66% for a temperature drop of 20°. We conclude that condensation of solids from the solar

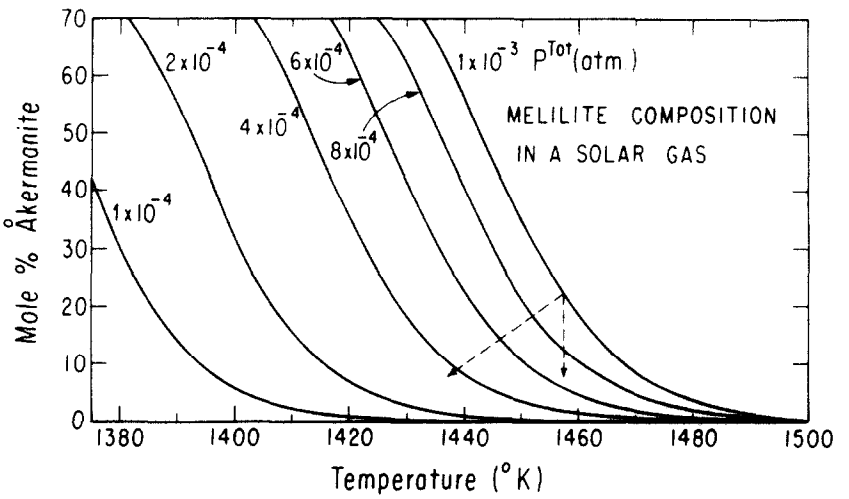

FIG. 11. Composition of melilite condensing from a gas of solar composition as a function of temperature and pressure. Arrows mark possible *P-T* trajectories that will result in reversely-zoned melilite crystals like the one in TS25F1, shown in Fig. 8.

nebular gas is clearly superior to crystallization of liquid droplets in explaining the melilite zoning in coarser-grained FTA's. The implication of this model of origin of these objects is that either the gas pressure fell in the region where they formed while the melilite was growing or condensation of melilite continued while their constituents were transported to nebular regions of lower pressure.

Evidence from non-uniform phase compositions

We saw above that the V_2O_3 content of spinel grains is highly variable within individual coarser-grained FTA's and concluded that this is not due to secondary alteration. The range of V_2O_3 contents of spinel grains in CG-11 (ALLEN *et al.*, 1978) is 0.25–1.2 wt.%, in TS24F1 0.75–2.25 wt.%, and in TS25F1 0.4–3.6 wt.%. Even within a single melilite host crystal, such as in TS24F1, different spinel grains vary in V_2O_3 content from 0.97–2.3 wt.%. In contrast, the range of V_2O_3 contents of spinel grains in the entire once-molten Type B1 inclusion studied by MACPHERSON and GROSSMAN (1981a) is 0.12–0.25 wt.% based on forty analyses. Furthermore, the compositions of different grains show no systematic relationship, either to the positions of the grains within coarser-grained FTA's or within individual melilite crystals, that could be interpreted in terms of liquid differentiation. These features indicate that the spinel grains did not equilibrate with one another during or since their formation and argue against the possibility that these inclusions were ever entirely molten or thoroughly metamorphosed. In addition, it is hard to imagine that each of these tiny spinel grains formed from its own liquid droplet having precisely the bulk composition of spinel. We suggest, rather, that these grains formed independently in space by direct condensation from the solar nebular gas. Spinel crystals of different composition could have equilibrated with the gas at slightly different temperatures and locations. Coarser-grained FTA inclusions then formed when these crystals, along with hibonite and perovskite grains, were brought together and incorporated by condensing melilite, followed by aggregation of the composite grains so produced.

In support of this general conclusion, there exists further evidence of internal disequilibrium in coarser-grained FTA's. WARK and LOVERING (1976, 1978) found that the compositions of refractory platinum metal nuggets within a single melilite crystal are similar to one another but differ significantly from those of nuggets in other melilite crystals in the same inclusion. From the descriptions of the inclusions studied by these workers, however, it is difficult to tell whether they are fluffy or compact Type A's. Similarly, STEELE and HUTCHEON (1979) showed that, while melilite, spinel and some hibonite in the inclusion Al 3529-45 fall along a common ^{26}Al-^{26}Mg isochron, other hibonite grains clearly lie above that isochron. Although models could be devised that explain this by exchange in an open system, another possibility is that the discordant hibonite never equilibrated with the other phases, implying that they originated in different nebular reservoirs from one another. Although this inclusion was described by MASON and TAYLOR (1982) as containing 20% fassaite and no hibonite, which would make it a Type B, our examination of their thin section revealed no fassaite but 20% hibonite along with other mineralogical and textural features that clearly place it in the coarser-grained FTA category.

IMPLICATIONS

One alternative to the suggestion that refractory inclusions condensed as solids from the solar nebular

gas (GROSSMAN, 1972; LATTIMER and GROSSMAN, 1978) is that they condensed as metastable liquids (BLANDER and FUCHS, 1975). The basis for the latter argument is that, in a low pressure gas, nucleation barriers for liquids are lower than those for crystals. The early proposal that some refractory inclusions probably solidified from melts was taken as support for such a model (BLANDER and FUCHS, 1975), even though that proposal is equally consistent with condensation of stable liquids (CLAYTON *et al.*, 1977) and with later melting of solid condensates. Although it is now generally accepted that Type B1 inclusions did indeed solidify from melts, recent work by PAQUE and STOLPER (1982) suggests that they crystallized slowly from partial melts and therefore that they could not have originated as metastable liquids. FTA's, on the other hand, were probably never molten and may be one component of the solid material that was melted to form B1's. There is thus mounting evidence against an origin for observed inclusions by condensation of metastable liquids.

Another alternative is that the inclusions are volatilization residues rather than early condensates (KURAT, 1970; WOOD, 1981). We have already seen, however, that the reverse zoning of FTA melilite cannot be explained by volatilization if a melt forms in the process. Furthermore, in the absence of a liquid, reversely-zoned melilite could only be produced during volatilization by creation of a diffusion profile in the existing crystals due to cation exchange across the gas-solid interface. This is exceedingly improbable because of the very slow rates of coupled exchange on tetrahedral sites. For these reasons, formation of coarser-grained FTA's as volatilization residues cannot be considered a viable hypothesis.

It is reasonably clear that neither whole FTA's nor constituent nodules of the coarser-grained ones were ever molten. We have also shown that, despite solid-state recrystallization which has affected these inclusions to varying degrees, the coarser-grained material remaining in many of them is probably a relic of vapor-solid condensation in the solar nebula.

To the extent that the latter interpretation is true, then the properties of coarser-grained FTA's have several implications for equilibrium condensation models. First, the phase $CaAl_4O_7$ is not a common condensate. Second, spinel condensed prior to melilite. Evidence for this conflict with existing condensation models has also been found in Murchison refractory inclusions (BAR-MATTHEWS *et al.*, 1982). The reason for spinel's early nucleation is unknown but it may be that spinel nucleates more readily than melilite, causing spinel to condense metastably prior to melilite.

The diversity of spinel compositions within each FTA and the existence of reversely-zoned melilite grains imply that each inclusion sampled material from a variety of physico-chemical environments within the solar nebula, implying transport of material over moderate distances.

Acknowledgements—We thank A. T. Anderson, J. R. Beckett, R. N. Clayton, J. S. Huebner, I. D. Hutcheon, G. Lofgren, J. V. Smith, E. Stolper and D. Walker for helpful discussions. We also thank John Beckett for providing unpublished data from experimental runs and James Lattimer for providing unpublished results of condensation calculations. This research was supported by the National Aeronautics and Space Administration through grants NGR 14-001-249 and NAG 9-54 and by the National Science Foundation through grant EAR-8218154.

REFERENCES

ALLEN J. M. and GROSSMAN L. (1978) Solar nebula condensation: Implications from Allende inclusion mineralogy (abstract). *Meteoritics* **13**, 383–384.

ALLEN J. M., GROSSMAN L., DAVIS A. M. and HUTCHEON I. D. (1978) Mineralogy, textures and mode of formation of a hibonite-bearing Allende inclusion. *Proc. Lunar Planet. Sci. Conf. 9th*, 1209–1233.

ALLEN J. M., GROSSMAN L., LEE T. and WASSERBURG G. J. (1980) Mineralogy and petrography of HAL, an isotopically-unusual Allende inclusion. *Geochim. Cosmochim. Acta* **44**, 685–699.

ALLIBERT M., CHATILLON C., JACOB K. T. and LOURTAU R. (1981) Mass-spectrometric and electrochemical studies of thermodynamic properties of liquid and solid phases in the system CaO-Al_2O_3. *J. Amer. Ceram. Soc.* **64**, 307–314.

BAR-MATTHEWS M., HUTCHEON I. D., MACPHERSON G. J. and GROSSMAN L. (1982) A corundum-rich inclusion in the Murchison carbonaceous chondrite. *Geochim. Cosmochim. Acta* **46**, 31–41.

BAR-MATTHEWS M., MACPHERSON G. J. and GROSSMAN L. (1979) An SEM-petrographic study of amoeboid olivine aggregates in Allende (abstract). *Meteoritics* **14**, 342.

BECKETT J. R. and GROSSMAN L. (1982) Melting experiments on Allende coarse-grained inclusion compositions (abstract). In *Lunar and Planetary Science XIII*, 31–32. Lunar and Planetary Institute, Houston.

BECKETT J. R., MACPHERSON G. J. and GROSSMAN L. (1980) Major element compositions of coarse-grained Allende inclusions (abstract). *Meteoritics* **15**, 263.

BISCHOFF A. and KEIL K. (1983) Catalog of Al-rich chondrules, inclusions and fragments in ordinary chondrites. *Univ. New Mexico Inst. Meteoritics Spec. Pub.* No. 22.

BLANDER M. and FUCHS L. H. (1975) Calcium-aluminum-rich inclusions in the Allende meteorite: evidence for a liquid origin. *Geochim. Cosmochim. Acta* **39**, 1605–1619.

CHINNER G. A. and SCHAIRER J. F. (1962) The join $Ca_3Al_2Si_3O_{12}$-$Mg_3Al_2Si_3O_{12}$ and its bearing on the system CaO-MgO-Al_2O_3-SiO_2 at atmospheric pressure. *Amer. J. Sci.* **260**, 611–634.

CHRISTOPHE MICHEL-LÉVY M., KURAT G. and BRANDSTÄTTER F. (1982) A new calcium-aluminate from a refractory inclusion in the Leoville carbonaceous chondrite. *Earth Planet. Sci. Lett.* **61**, 13–22.

CLAYTON R. N., ONUMA N., GROSSMAN L. and MAYEDA T. K. (1977) Distribution of the pre-solar component in Allende and other carbonaceous chondrites. *Earth Planet. Sci. Lett.* **34**, 209–224.

DAVIS A. M., GROSSMAN L. and ALLEN J. M. (1978) Major and trace element chemistry of separated fragments from a hibonite-bearing Allende inclusion. *Proc. Lunar Planet. Sci. Conf. 9th*, 1235–1247.

EL GORESY A., NAGEL K. and RAMDOHR P. (1978) Fremdlinge and their noble relatives. *Proc. Lunar Planet. Sci. Conf. 9th*, 1279–1303.

EL GORESY A., NAGEL K. and RAMDOHR P. (1979) Spinel framboids and fremdlinge in Allende inclusions: Possible sequential markers in the early history of the solar system. *Proc. Lunar Planet. Sci. Conf. 10th*, 833–850.

EL GORESY A., RAMDOHR P. and NAGEL K. (1980) A unique

inclusion in Allende meteorite: A conglomerate of hundreds of various fragments and inclusions (abstract). *Meteoritics* **15**, 286–287.

EL GORESY A., PALME H., YABUKI H., NAGEL K. and RAMDOHR P. (1983) A refractory inclusion from the Essebi (CM2) carbonaceous chondrite (abstract). In *Lunar and Planetary Science XIV*, 173–174. Lunar and Planetary Institute, Houston.

FEGLEY M. B. (1982) Hibonite condensation in the solar nebula (abstract). In *Lunar and Planetary Science XIII*, 211–212. Lunar and Planetary Institute, Houston.

GEE K. H. and OSBORN E. F. (1969) Phase equilibria at liquidus temperatures in a part of the system CaO-MgO-Al_2O_3-SiO_2: The system $Ca_2MgSi_2O_7$-$Ca_2Al_2SiO_7$-$CaMgSi_2O_6$-$CaAl_2Si_2O_8$. *Bull. Earth Min. Sci. Experiment. Station Penn. State Univ.*, No. 85, 23–51.

GROSSMAN L. (1972) Condensation in the primitive solar nebula. *Geochim. Cosmochim. Acta* **36**, 597–619.

GROSSMAN L. (1975) Petrography and mineral chemistry of Ca-rich inclusions in the Allende meteorite. *Geochim. Cosmochim. Acta* **39**, 433–454.

GROSSMAN L. (1980) Refractory inclusions in the Allende meteorite. *Ann. Rev. Earth Planet. Sci.* **8**, 559–608.

KEIL K. and FUCHS L. H. (1971) Hibonite [$Ca_2(Al, Ti)_{24}O_{38}$] from the Leoville and Allende chondritic meteorites. *Earth Planet. Sci. Lett.* **12**, 184–190.

KOEHLER M. F., BARANY R. and KELLEY K. K. (1961) Heats and free energies of formation of ferrites and aluminates of calcium, magnesium, sodium, and lithium. Bureau of Mines, Rept. Invest. RI 5711, U.S. Dept. Interior, Washington, D.C.

KORNACKI A. S. (1982) Major and trace element fractionations in fine-grained CAI's: Evidence for igneous differentiation during melting induced by partial distillation (abstract). In *Lunar and Planetary Science XIII*, 401–402. Lunar and Planetary Institute, Houston.

KURAT G. (1970) Zur Genese der Ca-Al-reichen Einschlüsse im Chondriten von Lancé. *Earth Planet. Sci. Lett.* **9**, 225–231.

LATTIMER J. M. and GROSSMAN L. (1978) Chemical condensation sequences in supernova ejecta. *The Moon and Planets* **19**, 169–184.

LINDSLEY D. H. (1968) Melting relations of plagioclase at high pressures. In *Origin of Anorthosite and Related Rocks* (Ed. Y. W. ISACHSEN), New York State Museum and Science Service Memoir 18, 39–46.

LOFGREN G. E. (1974) Temperature induced zoning in synthetic plagioclase feldspar. In *The Feldspars* (Eds. W. S. MACKENZIE and J. ZUSSMAN), 362–375. Manchester University Press, Manchester.

MACDOUGALL J. D. (1981) Refractory spherules in the Murchison meteorite: Are they chondrules? *Geophys. Res. Lett.* **8**, 966–969.

MACPHERSON G. J. and GROSSMAN L. (1979) Melted and non-melted coarse-grained Ca-, Al-rich inclusions in Allende (abstract). *Meteoritics* **14**, 479–480.

MACPHERSON G. J. and GROSSMAN L. (1981a) A once-molten, coarse-grained, Ca-rich inclusion in Allende. *Earth Planet. Sci. Lett.* **52**, 16–24.

MACPHERSON G. J. and GROSSMAN L. (1981b) Clastic rims on inclusions: Clues to the accretion of the Allende parent body (abstract). In *Lunar and Planetary Science XII*, 646–647. Lunar and Planetary Institute, Houston.

MACPHERSON G. J., GROSSMAN L., ALLEN J. M. and BECKETT J. R. (1981) Origin of rims on coarse-grained inclusions in the Allende meteorite. *Proc. Lunar Planet. Sci. Conf. 12B*, 1079–1091.

MACPHERSON G. J., BAR-MATTHEWS M., TANAKA T., OLSEN E. and GROSSMAN L. (1983a) Refractory inclusions in the Murchison meteorite. *Geochim. Cosmochim. Acta* **49**, 823–839.

MACPHERSON G. J., PAQUE J. M., STOLPER E. and GROSSMAN L. (1983b) The origin and significance of reverse zoning in melilite from Allende Type B inclusions. *J. Geol.* (Submitted).

MASON B. and TAYLOR S. R. (1982) Inclusions in the Allende meteorite. *Smithsonian Contrib. Earth Sci.*, No. 25.

NORD G. L. JR., HUEBNER J. S. and MCGEE J. J. (1982) Thermal history of a Type A Allende inclusion (abstract). *EOS* **63**, 462.

OSBORN E. F. and SCHAIRER J. F. (1941) The ternary system pseudowollastonite-akermanite-gehlenite. *Amer. J. Sci.* **239**, 715–763.

PAQUE J. M. and STOLPER E. (1982) Dynamic crystallization experiments on an average Ca-Al-rich inclusion composition (abstract). In *Papers Presented to the Conference on Chondrules and Their Origins*, 49. Lunar and Planetary Institute, Houston.

REED S. J. B. and WARE N. G. (1973) Quantitative electron microprobe analysis using a lithium drifted silicon detector. *X-Ray Spectrometry* **2**, 69–74.

STEELE I. M. and HUTCHEON I. D. (1979) Anatomy of Allende inclusions: Mineralogy and Mg isotopes in two Ca-Al-rich inclusions (abstract). In *Lunar and Planetary Science X*, 1166–1168. Lunar and Planetary Institute, Houston.

WARK D. A. and LOVERING J. F. (1976) Refractory/platinum metal grains in Allende calcium-aluminium-rich clasts (CARC's): Possible exotic presolar material? (abstract). In *Lunar and Planetary Science VII*, 912–914. Lunar Science Institute, Houston.

WARK D. A. and LOVERING J. F. (1977) Marker events in the early evolution of the solar system: Evidence from rims on Ca-Al-rich inclusions in carbonaceous chondrites. *Proc. Lunar Sci. Conf. 8th*, 95–112.

WARK D. A. and LOVERING J. F. (1978) Refractory/platinum metals and other opaque phases in Allende Ca-Al-rich inclusions (CAI's) (abstract). In *Lunar and Planetary Science IX*, 1214–1216. Lunar and Planetary Institute, Houston.

WOOD J. A. (1981) The interstellar dust as a precursor of Ca, Al-rich inclusions in carbonaceous chondrites. *Earth Planet. Sci. Lett.* **56**, 32–44.

YODER H. S., STEWART D. B. and SMITH J. R. (1957) Ternary feldspars. *Carnegie Inst. Wash. Yearb.* **56**, 206–214.